Space-Weather Monitoring, 12U CubeSat Design

Thomas Burghardt[1], Raymond Picquet[2], Katrina Ternus[3], Utsav Shah[4], Henry Mejias[5], Daynah Rodriguez[6], Sarah Ketchersid[7], Kiana Zarandi[8], Nicholas Juganu[9]
Embry-Riddle Aeronautical University, Daytona Beach, FL, 32114

As American and international space policy decisions continue to focus on crewed, lunar exploration missions, it will be necessary for space mission operators to prepare for significant risks that may occur outside of the Earth's magnetic field. Such risks include coronal mass ejections and other similar solar events, which can expose astronauts to dangerous radiation dosages. In a long-duration mission, ample warning is required to give astronauts time to seek shelter. However, the capabilities of current detection systems are limited and cannot identify active solar regions. This system can be improved by utilizing a Heliocentric satellite. The primary objective of this project is to design a 12U Heliocentric CubeSat, to utilize a white light coronagraph and extreme ultraviolet imager to provide real-time monitoring and alert capabilities for solar energetic particles.

Nomenclature

A	=	Albedo	S	=	Area
a	=	Semi-major Axis	T	=	Temperature
B	=	Magnetic Flux	z	=	Gear Tooth Number
D	=	Distance Between Earth and the Sun	α	=	Rotational Acceleration
d	=	Diameter	η	=	Efficiency
e	=	Eccentricity	θ	=	Angular Resolution
F	=	View Factor	λ	=	Wavelength
G	=	Antenna Gain	σ	=	Boltzmann's Constant
I	=	Moment of Inertia	τ	=	Torque
i	=	Inclination	Ω	=	Longitude of the Ascending Node
K	=	Controller Gain	ω	=	Argument of Periapsis
M	=	Gear Module			
m	=	Magnetic Dipole			
P	=	Power			
Q	=	Heat Energy			
q	=	Solar Flux			
R	=	Antenna Far-Field Line-of Sight			
r	=	Solar Radius			

[1]Undergraduate, Payload Subsystem Lead, AIAA Student Member
[2]Undergraduate, Project Lead, AIAA Student Member
[3]Undergraduate, Project Mission Planner, AIAA Student Member
[4]Graduate, Structural Design and Analysis Subsystem Lead, AIAA Student Member
[5]Undergraduate, Communications Subsystem Lead, AIAA Student Member
[6]Undergraduate, Command and Data Handling Subsystem Lead
[7]Undergraduate, Payload Subsystem Member, AIAA Student Member
[8]Undergraduate, Payload Subsystem Member, AIAA Student Member
[9]Undergraduate, Structural Design and Analysis Subsystem Member, AIAA Student Member

I. Introduction

The proposed 12U CubeSat concept, also known as the SCORCH (Solar and Coronal Observation of Radiation and Catastrophic Events to Humans) spacecraft, is designed to monitor potentially harmful solar events by identifying active regions, solar flares, coronal holes and Coronal Mass Ejections (CMEs). Observation of active regions can aid in predicting these hazardous phenomena.

These solar radiation behaviors affect the electronics of spacecraft and expose astronauts to detrimental levels of radiation. The active regions of the Sun, which include geomagnetic storms, have two solar sources: coronal holes and CMEs. Coronal holes, shown in Fig. 1, are large dark regions of lower-density plasma in the Sun's corona, which cause strong solar winds. CMEs, shown in Fig. 2, are regions of the Sun where significant amounts of plasma laced with magnetic field lines are ejected from the corona into the interplanetary atmosphere, reaching the magnetic field of the Earth. CMEs are blown away from the Sun, often during strong, long-duration solar flares and prominent solar eruptions[1]. Solar flares are higher-density regions of plasma and are more commonly observed than CMEs.

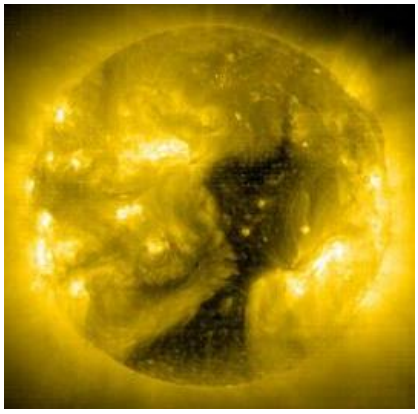

Figure 1. Coronal Hole Photo Taken on Jan. 8, 2002[2].

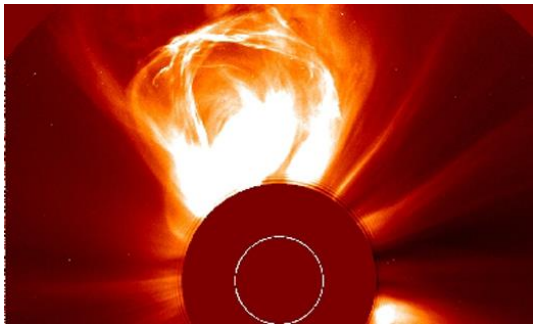

Figure 2. SOHO CME Photo Taken on Feb. 27, 2000[2].

Effective observation of these target solar behaviors enables the spacecraft to engage a warning system for humans working in space. This will be accomplished through two imaging methods: a white light coronagraph and a series of extreme ultraviolet filters. The coronagraph observes the sun in white light and uses an occulter to block the sun's primary disk, thereby providing an image of the corona. The EUV filters view the Sun's surface through different wavelengths, creating contrasting images that make active regions more distinct. In conjunction, these two data sources make SCORCH an asset in monitoring, analyzing and predicting solar events.

Several of the driving factors in the development of this spacecraft pertain to the optical systems. Both imagers must be able to resolve the Sun, which has a 0.5° angular diameter, or apparent size, as seen from Earth. In addition, both employ a Complementary Metal-Oxide Semiconductor (CMOS) imager as a pivotal part of the systems. Currently, SCORCH is targeting the usage of a Richey-Chretien Cassegrain reflector to serve as the optical system for the white light coronagraph due to its lack of spherical aberrations, coma errors, and use in similar satellite payload designs[3]. For the extreme ultraviolet imager, the optical system will consist of a focusing optic and filter wheel. Based on heritage data from the SOHO spacecraft, the proposed filter wheel is targeting 30.4, 28.4, and 17.1nm wavelengths[4].

II. Flightpath

For the SCORCH CubeSat to constantly check for space weather dangers, its flight path must allow a permanent view of the sun. To prevent obstruction from the Earth or Moon, it must be placed in a heliocentric orbit. Current NASA plans propose to deploy 6U and 12U CubeSats during Artemis II on a lunar flyby[5]. While we assume a launch during this mission, various orbital parameters do not currently exist. As a result, the launch location, date, and basic orbital path were assumed. The resulting flight path was analyzed using System Tool Kit (STK).

Initial NASA documents indicated an Artemis II launch of late 2022 or early 2023[6]. A specific date and time is not included, however, and is assumed to be February 1, 2023, at midnight. The Kennedy Space Center is the chosen launch selection. For the flight path simulation, the center of Earth is used as a reference point.

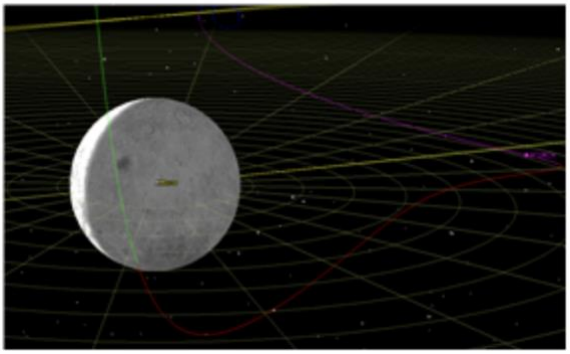

Figure 3. Flightpath in Lunar Vicinity.

During the flight, a low Earth orbit burn will send payloads towards the Moon. Six hours following the initial launch, SCORCH will reach an altitude of approximately 70,000km[7]. At this point, it will be ejected from the Orion Stage Adapter (OSA) and begin its detumbling maneuver. The control system will slow the rapid rotations of the satellite and solar panels will deploy. On February 10, 7:13 AM UTC, the CubeSat will be at its closest approach with the Moon, thus beginning the scientific phase of the mission as the SCORCH satellite starts tracking the Sun. Fig. 3 displays the cislunar trajectory, with the red curve representing the lunar approach, and the green curve showing the scientific phase trajectory. Despite the Moon's location and effect on the flight path, the SCORCH CubeSat will not lose sight of the sun.

After leaving cislunar space, the satellite will enter a heliocentric orbit. Using a solar reference frame, the initial distance is 1.4875+E8 km or 0.994 AU. The heliocentric flightpath also has a greater inclination than the Earth's orbit, as shown in Fig. 4. The pink curve represents the satellite, while the yellow curve displays the Earth's orbit. Also, other parameters of the flightpath were determined through STK and are displayed in Table 1.

Table 1. Heliocentric Orbital Parameters.

Variable	Value
a	1.5049+E8 km
e	0.0370
i	23.8197°
ω	266.12°
Ω	358.81°

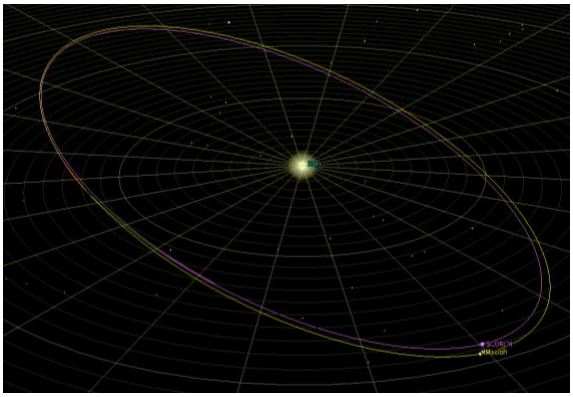

Figure 4. SCORCH Heliocentric Orbit.

III. Design Specifications

A. Payload

1. Design Overview

While the CubeSat is taking image data from the Sun, an internal filter wheel is powered by a motor. To reduce the rotation speed, torque from the motor is applied to the filter wheel via gears. Both of which will be custom constructed from Aluminum 7075, which is low-cost and responds minimally to thermal stress. The filter wheel and motor gear have a module of 0.32, a pressure angle of 20°, and a pitch of 5 mm. The reference, tip, and root diameters are determined using Equation (1), Equation (2), and Equation (3), respectively.

$$d_{RF} = zM \quad (1)^{8}$$

$$d_{TP} = d + 2M \quad (2)^{8}$$

$$d_{RT} = d - 2b \quad (3)^{8}$$

Table 2 shows the geometries of both gears and the calculated design diameters. The filter wheel is powered by a RH-U17-1 stepper motor, which has been selected due to its low cost and size, yet moderate performance. The motor has a mass of 4.04 g and rotates the filter wheel at a higher rotational velocity than the required rate to decrease measurement times.

Table 2. Payload Gear Variables.

Variable	Filter Wheel	Motor Gear
z	25	10
d_{RF}	80.0 mm	32.0 mm
d_{TP}	86.4 mm	38.4 mm
d_{RF}	72.0 mm	24.0 mm

The size of the other components in the optic system depends on the design requirements of the coronagraph. Its aperture diameter is calculated with Equation (4). The upper limit wavelength is assumed to be 700nm, while the sun's angular diameter, at roughly 1 AU, is equal to 0.5 rad.

$$d_{CO} = 1.22\left(\frac{\lambda}{\theta}\right) \tag{4}$$

Solving Equation (4) gives a design diameter of 9.79E-2 mm. This would imply that an optic with a diameter of 9.00E+3 mm at the same wavelength would be able to resolve objects with an angular size of 1.96", well within the pointing and science requirements for SCORCH's solar-observing requirements.

Another fundamental driver of the optical system relates to the occulter size for the coronagraph. It will have the same angular size as the Sun; however, the distance from the CMOS imager is vital to the functionality of the occulter, and consequently, the coronagraph. An estimate for the occulter can be obtained by calculating the arc length between the CMOS imager and occulter and using the Sun's angular diameter as the angle. Because the maximum distance between the imager and occulter in a 12U CubeSat is 20 cm, the occulter is 1.745 mm[7].

For the camera, a CMOS imager was selected due to its low price, low power usage, and high data transfer rate, compared to a charge-coupled device[9]. For the CubeSat, an Imperx C5180 CMOS 25 MP Cheetah Ruggedized camera is installed directly in-line with the telescope and a single filter in the wheel.

2. Data Collection

Data provided from the payload is directly taken from a C5180 CMOS 25 MP camera. The high-speed version of the camera has a maximum frame rate of 80 frames per second. The active pixel frame is 5120 x 5120 with each square pixel being 4.5 μm wide. The image data is accessed through 32 10-bit LVDS channels and transferred at a rate of 720 Mbps, per each Low Voltage Differential Signaling (LVSD) channel[10]. The image data is provided directly to the CCD image sensor and stored in the satellite's memory.

The exposure times of the camera must be compatible with both the coronagraph and extreme ultraviolet filters. For the SCORCH camera system, exposure times are similar to cameras on heritage vehicles. During the coronagraph experiment, the camera will be configured for a 5 second exposure time. This baseline coincides to design slides from the Next Gen Formation Flying Solar Coronagraph mission from NASA Goddard Space Flight Center[11]. The extreme ultraviolet imaging spacecraft calls for changing exposure times to adjust for imaging of different features. The ESA's SOHO used a CCD imager with a minimum exposure time of 140 milliseconds, which could be increased in 31-millisecond increments. A typical lowest exposure, which provides a baseline exposure time for SCORCH extreme ultraviolet imaging, was 1.5 seconds[11]. Heritage vehicle NOAA's GOES-12 Solar X-ray Imager focused on four classifications of solar regions: solar flare sites, active surface regions, coronal loops, and coronal hole boundary. When imaging these specific features, the exposure setting is adjusted accordingly. Images of solar flare sites utilized exposure times less than 10 milliseconds. Active region imaging is less than 100-millisecond exposures, coronal loop imaging used exposures less than 1 second, and coronal hoop boundaries used exposure times of 10 seconds or less[12]. An entire data cycle, which includes the turning of the filter wheel and exposure time will take 15 seconds.

3. Payload Subassembly

To showcase the payload and demonstrate the placement of its components, an exploded view diagram and corresponding legend can be seen in Fig. 5 and Table 3, respectively.

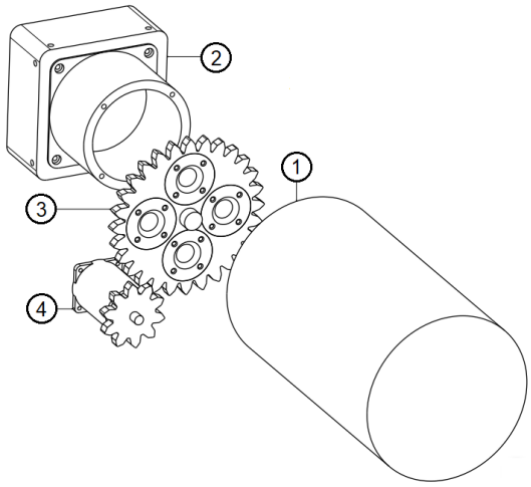

Table 3. Part Numbers in Payload Assembly.

1	Telescope
2	C5180 CMOS 25 MP Imager
3	Filter Wheel
4	RH-U17-1 Motor

Figure 5. SCORCH Scientific Payload.

B. Communications

The communications subsystem is composed of two main components: the transceiver and antenna. The transceiver used is the PULSAR-XTX, while the antenna is the PULSAR-XANT. Both of which can be acquired from AAC Clyde Space. For communicating between the ground station and the satellite, a frequency within the X-band range is used. In particular, the SCORCH CubeSat uses a radio frequency of 8.45 GHz ± 50 Hz, gain of 7.75 ± 0.5 dB, radio wavelength of 35.4 mm, and a transmission signal-to-noise ratio less than 20 dB[13]. The antenna transmitter power measurement is 40.76 dBm and is calculated using the Friis Transmission Equation[14], shown as Equation (5).

$$P_{tx} = \frac{P_{rx}}{G_{tx} + G_{rx} + 20\log_{10}\left(\left(\frac{\lambda}{4\pi R}\right)^{2}\right)} \quad (5)^{14}$$

The transmitter power can then be used to calculate the Effective Isotropically Radiated Power (EIRP) [14], shown as Equation (6), which is the actual power given to the transmitting antenna. This gives an EIRP of 48.51 dBm.

$$EIRP = P_{tx} + G_{tx} \quad (6)^{14}$$

Because the SCORCH CubeSat is transmitting images back to the ground station, the downlink rate is large and is approximated to be in a range of 10-50 Mbps[15]. Communication with the satellite must also be reliable and consistent at large distances, making a high gain antenna necessary.

C. Command and Data Handling

The Command and Data Handling (CDH) subsystem includes an ISIS On-Board flight computer (OBC) as its central processor to handle major satellite operating calculations. It operates KubOS Linux as its operating system and C as its programming language, which is consistent for the other computing devices in the SCORCH CubeSat. The OBC features a 400MHz 32-bit ARM9 processor and a daughterboard architecture. The overall architecture is centralized, where all subsystems are connected to the main processor. The SCORCH command system is shown in Fig. 6. Since the architecture is centralized, power consumption and cost are low.

The OBC contains a built-in external watchdog timer, real-time clock, an image sensor interface, and four storage units. The external watchdog timer autonomously resets the operations of the CubeSat to prevent software failures. Other components in the OBC include a real-time clock, an image sensor interface, and four storage units. These units store memory and are briefly described in Table 4.

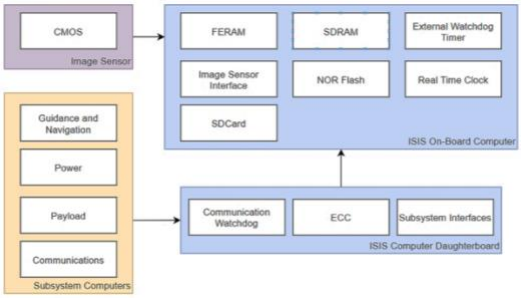

Figure 6. Command & Data Handling Architecture

The daughterboard contains three components: Error-Correcting Code memory (ECC), subsystem interfaces, and communication watchdog. The ECC is a computer data storage that detects and corrects internal data corruption such as flipping bits. Subsystem computational devices such as the Guidance, Navigation, and Control (GNC) computer, connects directly to the OBC. The final component is an additional watchdog.

Table 4. Memory Storage Devices.

FERAM	256kB Critical Data Storage
SDRAM	64MB Volatile Memory
NOR Flash	1 MB Code Storage
SD Card	2x2 GB for Fail Safe Data Storage

D. Structural Design and Analysis

The structural bus of the CubeSat must not only house and protect all internal components during the mission but survive the intense body loads applied during the launch. For the SLS, a maximum acceleration of 3.8 g's will be applied[7]. The OSA, which carries the SCORCH CubeSat as a payload, keeps the satellite at a pitch angle of 30°. The bus must also fit within a launch envelope of 20 x 20 x 30 cm[7]. Along with surviving the initial launch acceleration, the bus must survive vibration and vacuum tests. All three can be simulated in Solid Edge supported by NX NASTRAN. The frame is comprised of high strength - low weight material, Aluminum 6061-T6, which has a yield stress of 248.211 MPa[16]. Four, thick rails make up the long edges of the bus and are used to prevent undeployed solar panels from striking the OSA walls. Thin, rectangular frames connect the rails and a circular subsection at the front is cut out to give the telescope clearance. Fig. 7 shows a trimetric view of the bus design.

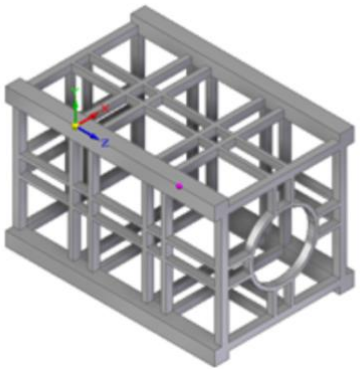

Figure 7. Trimetric View of CubeSat Bus.

The SCORCH CubeSat bus was analyzed using Solid Edge. Any surfaces of the CubeSat which make contact with the OSA were fixed in the simulation. An interior mass of 20kg is placed in the bus to simulate payload weight acting on the exterior frame. 20kg is also the maximum allotted mass for a 12U CubeSat in the SLS. The frame's stress and maximum deflection when the body force is applied are shown in Fig. 8 and Fig 9. respectively.

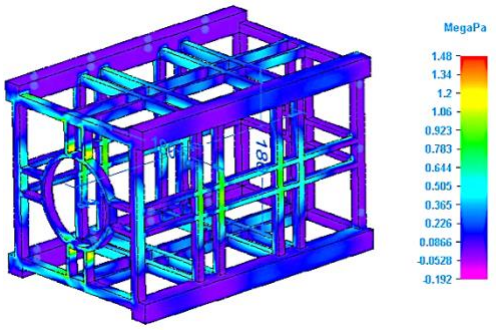

Figure 8. CubeSat Bus Stress under Body Load.

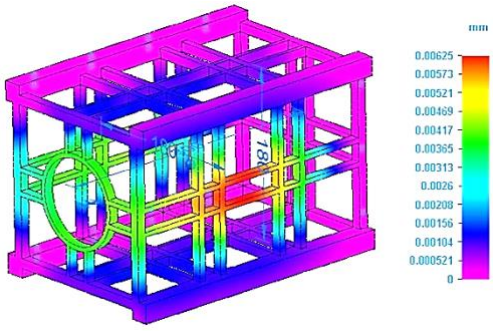

Figure 9. CubeSat Deflection under Body Load.

According to the results, the bus undergoes the most stress in the beams which connect to the circular telescope frame. The greatest deflection occurs at the center of the bus. Although the simulation shows some weak points in the design, the stress is significantly lower than the yield stress of Aluminum 6061. The deflection is also too small to be significant.

A final analysis is done after assembling all the components shown in Fig. 10 along with solar panels, to understand the actual behavior of the CubeSat under the maximum acceleration applied. After the analysis, it can be said that the

total deflection is significantly less than the overall dimension of the CubeSat and poses no threat to the components during the launch.

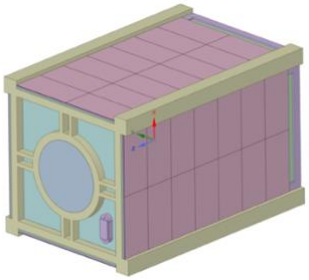

Figure 10. Isometric View of Complete CubeSat.

E. Thermal Control

To ensure the CubeSat will not become damaged due to extreme radiative heat absorption, thermal analysis is incorporated into the design. This is especially important considering the SCORCH CubeSat will be constantly Sun-pointing. Currently, the analysis does not consider all subsystems' placement and heating. To determine the range of temperatures of the bus, the temperature differences were calculated using Equation (7).

$$S_{SOL}q_{SOL} + FS_{SAT}\sigma\bar{T}_E^4 + FS_{SAT}Aq_{SOL} + Q = S_{SAT}\sigma\bar{T}^4 \quad (7)^{17}$$

Equation (8) solves for the Earth's equilibrium temperature to determine the amount of heat added to the bus from the Earth's albedo.

$$T_E = T_{SOLAR}\sqrt[4]{1-A}\sqrt{\frac{r_{SOLAR}}{2D}} \quad (8)^{17}$$

Equations (7) and (8) can be combined to form Equation (9), solving for the equilibrium temperature of the bus.

$$\bar{T}^4 = \frac{q_S}{\sigma}\left(\frac{S_{SOL}}{S_{SAT}} + FA\right) + FT_E^4 \quad (9)^{17}$$

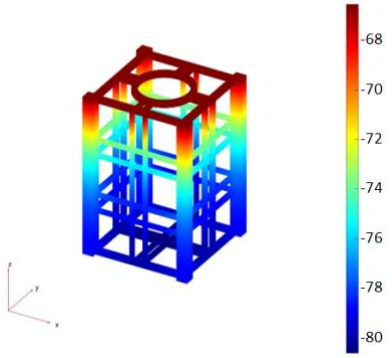

Figure 11. Steady-State Temperature (°C).

By meshing the bus in MATLAB and solving for a steady-state of the system, Fig. 11 is produced, showing the temperature gradients. It is expected that the bus will increase in temperature when an external skin is added to the bus and when the internal components are added. Furthermore, devices such as flight computers produce heat, which can be transferred throughout the aluminum frame.

Exterior components such as the solar panels are expected to add negligible heat to the bus. Heat could be added to the bus through the expenditure of excess energy produced by the solar panels. In the event of overheating, however, an active thermal system can be used to distribute energy through radiators.

F. Power

The power subsystem is formed by three primary sections: generation, distribution, and storage elements. Power generation is carried out by a set of four 16 x 28 cm solar panels placed on each 20 x 30 cm surface on the CubeSat. During deployment, each panel rotates about a hinge at the fore-edges of the bus until the surfaces are normal to the Sun-pointing direction.

The deployment takes place using the "Mini Frangibolt" manufactured by Ensign-Bickford Aerospace and Defense (EBAD). This device is a non-explosive bolt-breaking actuator designed with different configurations for small-scale aerospace projects. The CubeSat will be using the "FD04" shown in Fig. 11, an 8g device capable of supporting a maximum load of 667N. This actuator operates within 50-70° C, requires 6-8V DC and draws 9 watts of power. The solar panel will be spring-loaded and bolted down into the frangibolt with .036 kg m of torque before deployment. Upon activation, the device will apply torque to the bolt until it exceeds its tensile strength ultimately breaking the bolt and releasing the solar panel from its locked down position[18].

Figure 11. Mini Frangibolt actuator.

Distribution of power is handled by a modular, off-the-shelf system produced by ISISPACE consisting of a battery, conditioning, and distribution units. The storage system is composed of four Lithium-Ion battery cells.

Solar panels are employed in SCORCH's design as a result of the long-term power requirement imposed by the mission lifespan. Due to a lack of commercially available, space-rated solar panels fitting the launch envelope requirement, the SCORCH CubeSat employs Alta Devices triple-junction gallium arsenide solar cells, which produce 1.2W per 40 x 80mm cell[19]. To size the solar panels, the power draw of each subsystem was added together and organized in Table 5.

Table 5. Subsystem Power Draw

Subsystem	Power (W)	Distribution (%)
Payload	22.6	37.92
Communications	22	36.91
CDH	0.004	0.007
Structural Design	0	0
Thermal Control	0	0
Power	9	15.10
GNC	6	10.07
TOTAL	59.60	100

Because some energy may be lost between the solar panels and the CubeSat systems due to heat, it is assumed the satellite will have a path efficiency of 85%[3]. The required power draw is calculated through Equation (10).

$$P_R = \frac{P_S}{\eta_P} \tag{10}$$[3]

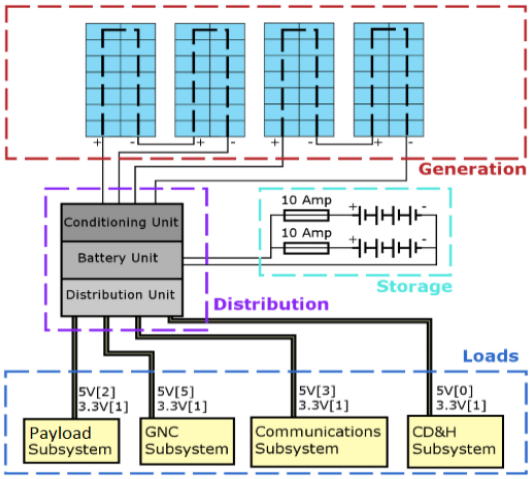

Figure 12. Power Subsystem Component Layout.

This raises the total potential power draw from 59.6W to 70.1W. As a result, 56 solar cells were selected for the design, to form four equally sized solar panels. Combined, they produce 67.2W. The minor discrepancy is allowable as peak loading will not be reached at any point in the mission. To cut down on weight and volume, peak power usage was minimized by analysis of which systems would be operating during specific phases of the mission. A four-cell lithium-ion battery solution was identified as a feasible option when identifying the total power that would be required for SCORCH to operate at capacity during all phases of flight. Due to the complexity of conditioning and distributing power, an existing modular commercial solution is employed. A 4-channel input, 24 channel output device, which is in line with system requirements, has been selected to form the core of the power system.

With primary components of the power subsystem combined, the design of the subsystem is shown in Fig. 12.

G. Guidance, Navigation, and Control

Due to high required pointing accuracy for the payload, the SCORCH CubeSat will utilize a variety of components to create a 3-axis stabilization control system. This requires at least three reaction wheels, detumbling components, attitude sensors, and more. The CubeSat must also have enough reaction control devices to reorient itself after a perturbance or other resistance torques are applied. The greatest of which occurs during the detumbling maneuver after the CubeSat is ejected from the OSA. The satellite's reaction wheels can be sized by calculating the required rotational acceleration and determining the moment of inertia.

$$\tau = I\alpha \quad (11)^{20}$$

The SCORCH CubeSat is assumed to spin at a rotational velocity of 5 rotations a minute, about the axis with the greatest moment of inertia in a worst-case scenario. For orienting the spacecraft properly, three CubeWheel S's, with 2.30E-3 Nm of torque each will be utilized.

Although the reaction wheels may be effective in slowing down the spacecraft during detumbling, they will slowly begin storing momentum overtime[3]. This can lead to momentum saturation. Because the CubeSat is well within the Earth's magnetic field during detumbling[7], it can utilize magnetorquers for momentum dumping. In the case of the SCORCH CubeSat, a HMC2003, 3-axis magnetic sensor and 3 NCTR-M012 magnetorquers will be included. To determine the gain of the torquers, Equation (12) is used.

$$m = -K\dot{B} \quad (12)^{20}$$

Equation (13) is used to calculate the torque produced by the magnetic field and torquers.

$$\tau = m \times B \quad (13)^{20}$$

In addition to actuators, two additional sensors will be used. These include a nanoSSOC-A60 analog sun sensor to keep the CubeSat Sun-pointing and a STIM202 gyro to measure rotations about all axes. An AT91SAM9260 microcontroller will serve as a flight computer. A diagram of the control system components is shown in Fig. 14.

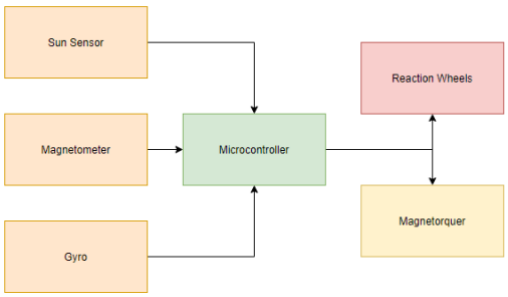

Figure 14. GNC Subsystem Component Layout.

The reaction wheels will be placed on the principal axes, which intercept the Center of Mass (COM). The distance from the approximated COM of the CubeSat from the structural frame COM and moments of inertia are shown in Table 6. The X-axis is set as the sun-pointing direction.

These variables only consider immovable components such as the structural bus, scientific payload, and solar panels. Other components including batteries, the OBC, etc. are not considered and can be placed in the CubeSat accordingly to move the satellite COM closer to the structural frame COM.

Table 6. SCORCH CubeSat Control Variables

Axis	COM (mm)	I (kg·m^2)
X	0.568	0.073
Y	2.626	0.071
Z	-2.331	0.049

The dynamics of the motion of the satellite are defined by Euler's equations of motion as a two-part two-body problem. The non-linear system of equations is adjusted for every transfer of orbit, change of frame of reference, and initialized based on the orbital parameters, in the computer program. Apart from satellite body reference dynamics, the sun sensors, solar panels, and antennas are modeled and programmed separately to point in the direction of the sun and the earth, respectively. This system is represented as a state space and linearized over 0.1 second time step and the solution to the linear system is used as the initial and subsequent current state estimates to propagate through the

continuous time dynamic model and discrete time sensor data. The covariance of estimates and the Kalman gain used to construct the control law are updated through every time step based on the sensor measurements with measurement matrix H = [1 1 1 0 0 0] and discrete time update laws. The Kalman filter is so implemented to achieve the accuracy of expected position and velocity with the standard deviation of 0.08 such that the outputs from gyros are used as the sensor feedback for the comparison of estimates with the true state of the satellite and the computationally efficient code improves the covariance with time.

The alternative solutions to design the control for proposed dynamics are model-based adaptive control for real-time integration as well as state and gain estimation. This control is however computationally expensive and slower as compared to the Kalman filter. The non-linear least squares approach is the most suitable mean of modeling and controlling the non-linear satellite dynamics given proper stabilization criteria of the body based on its mass properties.

The implementation of this dynamic model and control is planned to bring about using Simulink real-time workshop and auto-code generator. The actuators are activated with the appropriate voltage using the modeled state-flow logic developer in Simulink.

IV. Conclusion

With the inevitable crewed exploration beyond Low Earth Orbit, developing methods of detecting or mitigating radiation risks to astronauts will become a priority. Creating architecture capable of predicting space weather risks, such as CMEs or coronal holes, will significantly decrease the present risk. The SCORCH CubeSat is designed to act as not only part of this architecture, but as an alert system. Although the preliminary design of the satellite is completed, additional structural and thermal testing will be required to make it flight-ready. Vacuum, vibration, radiation, and magnetic testing can also be undertaken with fabricated components, with the end goal being to deploy a network of these spacecraft to monitor solar weather.

Acknowledgments

The AIAA student branch at Embry-Riddle Aeronautical University in Daytona Beach, FL and the following people are thanked for their involvement with and continued support of the S.C.O.R.C.H. design project going back to 2019.

Advisors
Dr. Jennifer Smith
Dr. Dongeun Seo
Brennan McCann

Leadership
Andrew Beres
Sean Harrison
Alex Horvath
Raymond C. Picquet
Katrina Ternus
Paul Winner

Payload Subsystem
Tobey Bautista
Thomas Burghardt
Michael Daven
Sarah Ketchersid
Kiana Zarandi

Guidance, Navigation, & Control Subsystem
Rasika Kale
Mustapha Khawaja
Arthur Shune

Structural Design & Analysis Subsystem
Asa Barringer
Rubendry Cruz
Joshua Jones
Nicholas Juganu
Utsav Shah
Harry Shrager
Michael Tomaso

Command & Data Handling Subsystem
Kyle Overton
Daynah Rodriguez

Thermal Control Subsystem
Taylor Stark

Power Subsystem
Josephine Moore
Venesh Pershaud
Jovon Thomas

Communications Subsystem
Grant Mathews
Henry Mejias

References

[1]Hill, S. M., Pizzo, V. J., Balch, C. C., Biesecker, D. A., Bornmann, P., Hildner, E., ... & Vickroy, J. (2005). The NOAA Goes-12 solar X-ray imager (SXI) 1. Instrument, operations, and data. Solar Physics, 226(2), 255-281.

[2]Garner, R. (2017). Solar Storm and Space Weather – Frequently Asked Questions. [online] NASA TV. Available at: https://www.nasa.gov/mission_pages/sunearth/spaceweather/index.html

[3]Wertz, J. R., & Larson, W. J. (1991). Space mission analysis and design. Dordrecht: Kluwer Academic Publishers.

[4]Delaboudiniere, J. P., Artzner, G. E., Brunaud, J., Gabriel, A. H., Hochedez, J. F., Millier, F., ... & Kreplin, R. (1995). EIT: extreme-ultraviolet imaging telescope for the SOHO mission. In The SOHO Mission (pp. 291-312). Springer, Dordrecht.

[5]Hill, D. (2019). NASA's CubeSat Launch Initiative Opens Call for Payloads on Artemis 2. [online] NASA TV. Available at: https://www.nasa.gov/feature/nasa-s-cubesat-launch-initiative-opens-call-for-payloads-on-artemis-2-mission

[6]Hambleton, K. (2019). NASA's Deep Space Exploration System is Coming Together. [online] NASA. Available at: https://www.nasa.gov/feature/nasa-s-deep-space-exploration-system-is-coming-together

[7]NASA. (2019). Artemis 2 Secondary Payloads 6U &12U Potential CubeSat Accommodations. [PDF] NASA Marshall Space Flight Center.

[8]Basic Gear Terminology and Calculation. (n.d.). Retrieved from https://khkgears.net/new/gear_knowledge/abcs_of_gears-b/basic_gear_terminology_calculation.html

[9]Chromey, F. R. (2017). To measure the sky: an introduction to observational astronomy (2nd ed.). Cambridge: Cambridge University Press.

[10]Shah, N., Davila, J., Chamberlin, P., Calhoun, P. Next-Generation Formation Flying Solar Coronagraph. Proceedings of iCubeSat 2014, 3rd Interplanetary CubeSat Workshop, Pasadena, CA, USA, May 27-28, 2014

[11]Delaboudiniere, J. P., Artzner, G. E., Brunaud, J., Gabriel, A. H., Hochedez, J. F., Millier, F., ... & Kreplin, R. (1995). EIT: extreme-ultraviolet imaging telescope for the SOHO mission. In The SOHO Mission (pp. 291-312). Springer, Dordrecht.

[12]GOES I-M Data Book (1996) NASA Goddard Space Flight Center, Greenbelt, MD, U.S.A., p. 196.

[13]AAC Clyde Space, "PULSAR-DATA" Datasheet, Website PULSAR-DATA. (2020).[PDF] AAC-Clyde Space. Available at: https://www.aac-clyde.space/assets/000/000/105/PULSAR-DATA_original.pdf?1565702890.

[14]Shaw, J. (2013). Radiometry and the Friis Transmission Equation. [PDF] American Journal of Physics.

[15]Kim, Y., Daly, R., Kim, J., Fallin, C., Lee, J. H. Flipping Bits in Memory Without Accessing Them: An Experimental Study of DRAM Disturbance Errors. [PDF] Carnegie Mellon University.

[16]Department of Defense. (2003)) Metallic Materials and Elements for Aerospace Vehicle Structures: MIL-HDBK-5J. [PDF].

[17]Dinh, Dai. Thermal Modeling of Nanosat. Master's Theses. 4193. https://doi.org/10.31979/etd.cx59-auuj

[18]"TiNi™ Mini Frangibolt® Actuator," *Ensign-Bickford Aerospace & Defense* Available: https://www.ebad.com/tini-mini-frangibolt/#erm-e250749d-007b.

[19]Alta Devices. (2017). Lightweight, High-Performance Solar Cells for High Power-to-Weight and Deployable Solar Arrays. [PDF] Hanergy.

[20]Gravdahl, J., Eide, E.,Skavhaug, A., Fauske, K., Svartveit, K., & Indergaard, F. (2003). Three Axis Attitude Determination and Control System for a Pico-Satellite: Design and Implementation. Norwegian University of Science and Technology.